Published in final edited form as:
Invest Ophthalmol Vis Sci. 2007 August ; 48(8): 3796–3804.

Manganese-Enhanced MRI Studies of Alterations of Intraretinal Ion Demand in Models of Ocular Injury

Bruce A. Berkowitz[1,2], **Robin Roberts**[1], **Hongmei Luan**[1], **David Bissig**[1], **Bang V. Bui**[3], **Marius Gradianu**[1], **David J. Calkins**[4], and **Algis J. Vingrys**[3]

1 *Department of Anatomy and Cell Biology, Wayne State University, Detroit, Michigan*

2 *Department of Ophthalmology, Wayne State University, Detroit, Michigan*

3 *Department of Optometry and Vision Sciences, University of Melbourne, Victoria, Australia*

4 *Department of Ophthalmology and Visual Sciences, Vanderbilt University, Nashville, Tennessee*

Abstract

Purpose—To provide proof-of-concept that the extent of intraretinal manganese uptake after systemic $MnCl_2$ injection, detected with manganese-enhanced MRI (MEMRI), assesses alterations in intraretinal ion demand in models of ocular insult.

Methods—In Sprague–Dawley rats, retinal ion demand and thickness were measured from MEMRI data collected before, 4 hours after, or 1, 3, and 7 days after intraperitoneal injection of $MnCl_2$. Choroidal contribution or blood-retinal barrier permeability surface area product (BRB PS′) was determined using MRI after Gd-DTPA injection. Ocular injury was evaluated 24 hours after intravitreal injection of phosphate-buffered saline (PBS, vehicle) or PBS + ouabain, or after intraperitoneal injection of sodium iodate. Manganese retinal toxicity was assessed by comparing full-field, white-flash electroretinographic (ERG) data obtained before and after systemic $MnCl_2$ administration. Rat choroidal thickness was measured from cross-sections prepared from paraformaldehyde-perfused adult rats.

Results—Comparing pre– and post–Gd-DTPA images demonstrated minimal choroidal contribution to intraretinal analysis. Intraretinal signal intensity returned to baseline by 7 days after $MnCl_2$ injection. After ouabain injection, receptor and postreceptor uptake of manganese were subnormal ($P < 0.05$). After sodium iodate exposure, intraretinal manganese uptake was supernormal ($P < 0.05$) and did not increase with increasing BRB PS′. ERG data did not show any effect of $MnCl_2$ on photoreceptor a-wave and postreceptor b-wave relative to baseline at either observation time.

Conclusions—MEMRI measurements of uptake of systemically administered and nontoxic doses of manganese appear to be a powerful approach for measuring alteration in intraretinal ion demand in models of ocular injury.

Electroretinographic measurements and ocular coherence tomography (OCT) are useful approaches for inferring in vivo aspects of retinal function during normal development and dysfunction in diseases such as diabetic retinopathy and retinal degeneration. However, these methods are limited by low spatial resolution or are used after-the-fact and thus indirectly indicate loss of function from the extent of retinal thinning. Recent efforts to address these problems have focused on the use of the organic cation agmatine, the natural decarboxylation

Corresponding author: Bruce A. Berkowitz, Department of Anatomy and Cell Biology, Wayne State University School of Medicine, 540 E. Canfield, Detroit, MI 48201; baberko@med.wayne.edu.

Disclosure: **B.A. Berkowitz**, None; **R. Roberts**, None; **H. Luan**, None; **D. Bissig**, None; **B.V. Bui**, None; **M. Gradianu**, None; **D.J. Calkins**, None; **A.J. Vingrys**, None

product of arginine, to study NMDA and a subset of AMPA receptor/channel complexes.[1] This approach provides high-resolution images of alternations in glutamatergic drive but only from small regions of retina ex vivo.[1–3] High-speed, ultrahigh-resolution OCT has been used in rats in vivo to measure changes in average reflectivities of photoreceptor outer segments in response to various lighting conditions.[4] However, the reflectance changes continued well after the stimulus, thus raising questions about the physiologic origins of the change and its possible application to retinopathy.[4] One potentially useful alternative is MRI, which allows in vivo imaging of retinal anatomy and cellular activity involved with retinal function but without optical interference.[5–8]

Normal cellular activity supporting retinal function and healthy vision includes photoreceptor transduction, retinal neurotransmitter release, regulation of gap-junction conductance, and modulation of postsynaptic potentials in retinal ganglion cells and is strongly dependent on proper cellular demand for ions such as calcium. Furthermore, changes in retinal ion demand have been reported early in the course of diseases such as diabetic retinopathy[9–11] and retinal degeneration.[2,3] Thus, measurement of demand for ions in vivo could provide additional useful information about retinal cell activity.

We have been investigating the use of systemically administered $MnCl_2$ as a probe of retinal layer–specific activity in vivo. Manganese ion (Mn^{2+}) is a surrogate for ions such as calcium, which play an important role in cellular activity,[12] and is an essential trace element[13] and a strong MRI contrast agent.[12] High-resolution manganese-enhanced MRI (MEMRI) of the retina has been shown to robustly measure light adaptation-dependent manganese uptake in different retinal layers in rats in vivo.[5] However, whether MEMRI can measure pathophysiologic alterations in retinal ion demand remains unclear. One potential limitation to the resolution of intensity changes in retinal layers is the possible contribution of signal from the choroidal circulation.

Systemically administered $MnCl_2$ at moderate concentrations does not impair the outward behavior of rodents[14] and, at 1 month after injection, did not alter retinal thickness or blood-retinal barrier (BRB) integrity.[5] Although such data provide indirect evidence that systemic $MnCl_2$ is not toxic, more direct evaluation of possible short-term changes in retinal function is required to confirm such a conclusion.

To address the above issues, we first used a vascular contrast agent (Gd-DTPA) to enhance the choroidal circulation and so investigate whether it substantially alters the estimate of total retinal thickness on MEMRI examination. In addition, we measured intraretinal MEMRI signal intensities as a function of time after $MnCl_2$ injection and in two models of ocular injury, metabolic inhibition through intravitreal injection of ouabain and damage to the retinal pigment epithelium layer (RPE) from systemic sodium iodate injection.[15–17] Finally, we evaluated the potential toxicity of our standard dose of systemically administrated $MnCl_2$ using modern electroretinographic (ERG) methods.

Methods

Animals were treated in accordance with the National Institutes of Health Guide for the Care and Use of Laboratory Animals and the ARVO Statement for the Use of Animals in Ophthalmic and Vision Research.

Groups

Age-matched controls and experimental female Sprague–Dawley rats (200–350 g) were used. All rats were housed and maintained in normal 12-hour cycled laboratory lighting. Rats were then maintained in darkness for 20 hours before manganese injection. For dark-adaptation

studies, all procedures (e.g., weighing rat, injecting $MnCl_2$, anesthesia for MRI, and MRI examination) were performed under dim red light or in darkness. For light adaptation studies, rats were light adapted for 10 to 20 minutes before injection of $MnCl_2$. In all cases, $MnCl_2$ was administered as an intraperitoneal injection (44 mg/kg) in the right sides of awake rats. Rats were maintained in dark or light conditions (as appropriate) for another 3.5 hours and then were anesthetized for MEMRI evaluation.

Histology

For histologic measurements of choroidal thickness, four adult Brown Norway rats were transcardially perfused with 4% paraformaldehyde. We used this species for ease of visualizing the pigmented choroid. After fixation, the eyes were removed, embedded in paraffin, and cross-sectioned serially at 10-μm intervals.

MRI Data Acquisition

High-Resolution MRI—Immediately before MRI experiment, rats were anesthetized with urethane (terminal study, 36% solution, intraperitoneally, 0.083 mL/20 g animal weight, prepared fresh daily; Aldrich, Milwaukee, WI) or ketamine/xylazine/acepromazine (time course study, 60, 6, and 1.5 mg/kg, respectively). To maintain the core temperature, a recirculating heated water blanket was used. Rectal temperatures were continuously monitored throughout each experiment, as previously described.[18] MRI data were acquired (4.7 T Avance system; Bruker Medical Inc., Billerica, MA) using a two-turn transmit/receive surface coil (1-cm diameter) placed over the eyes. Images were acquired using an adiabatic spin-echo imaging sequence (repetition time [TR] 350 seconds; echo time [TE] 16.7 ms; number of acquisitions [NA] 16; sweep width 61,728 Hz; matrix size 256 × 512; slice thickness 600 μm; field of view 12 × 12 mm^2; 23 minutes/image).[19] A single transverse slice through the center of the eye (based on sagittal localizer images collected using the same adiabatic pulse sequence as above) was obtained for each rat.

Choroid/Gd-DTPA—Light-adapted rats were imaged with MEMRI using the same high-resolution parameters described above before and immediately after injection of a bolus of Gd-DTPA (0.3 mmol/kg; Magnevist; Bayer HealthCare Pharmaceuticals, Leverkusen, Germany) into the tail vein. To ensure minimal movement between pre– and post–Gd-DTPA images, rats were anesthetized with urethane as described, paralyzed with pancuronium bromide (1.4 mg/kg, intravenously), and mechanically ventilated. Only this group of rats underwent the ventilation procedure.

Ouabain—Rats were injected intravitreally with vehicle (n = 5, phosphate-buffered saline [PBS]) in one eye and ouabain (n = 5, 3 μL of a 0.55 mM solution) in the contralateral eye. After recovery, the rats were placed in a dark room. The next day both eyes of dark-adapted rats were sequentially studied by MEMRI, as described above. A previous study had demonstrated that this dose of ouabain suppresses retinal function for 24 hours after injection (Weymouth AE, et al. *IOVS* 2004; 45:ARVO E-Abstract 1349).

Sodium Iodate—Conscious rats (n = 8) were given 30 mg/kg sodium iodate (Sigma, St. Louis, MO) intraperitoneally 24 hours before the MRI examination. After this injection, rats were placed in a dark room overnight. The next day rats were light adapted for 20 minutes before they were given manganese and subsequently were studied by MEMRI (vide supra) and by Gd-DTPA (vide infra). Previous studies have demonstrated that this dose of sodium iodate can produce BRB damage within 24 hours of injection.[16,17] Uninjected rats (n = 10) were used as controls. After the MEMRI data were collected, dynamic-contrast enhanced MRI data were collected, as previously described, through a spin-echo imaging sequence (repetition time [TR], 1 second; echo time [TE], 22.7 ms; number of acquisitions [NA], 1; matrix size, 128 ×

256; slice thickness, 1 mm; field of view, 32 × 32 mm^2; sweep width, 25,000 Hz; 2 minutes/image).[17] Twelve sequential 2-minute images were acquired as three control images before injection of contrast agent and nine images during and after a 6-second Gd-DTPA bolus injection. In other words, images were acquired for up to 18 minutes after injection of Gd-DTPA.

Data Analysis

Histology—Centrally located sections from the paraffin-embedded eyes were stained with hematoxylin and eosin and photographed under a 60× oil-immersion objection.

From a series of micrographs, 30 to 40 measurements of choroidal thickness were made from each eye (ImagePro software; Media Cybernetics, Bethesda MD). All measurements were within the central 0.4- to 1-mm interval of retina on either side of the optic nerve head. We excluded measurements from any region that contained artifactual separation of the choroid from the retinal pigment epithelium or obvious tearing or distension from the perfusion.

Choroid/Gd-DTPA—Choroidal thickness was assessed in two ways: by taking the difference in total retinal thickness (vide infra[5]) for pre– and post–Gd-DTPA images and by analyzing the difference images for each rat. The difference image was generated using in-house written software to map the in situ image into a linear representation for each retina. First, the vitreoretinal border and optic nerve were manually defined. Using the center point of each highlighted pixel, a straight line was fit to the optic nerve, and a sixth-order polynomial was fit to the vitreoretinal border. The intercept between the vitreoretinal border and the optic nerve regions-of-interest served as the origin of the linearized image. Along the polynomial, 50,000 evenly spaced values were then chosen by the program, and distances between each point and the one adjacent were calculated. With these distance measurements, fine-grained linear approximations of distances along the polynomial are available. For each of the 50,000 values, a line normal to every 50th is drawn, and intensity values along the normal were extracted and reconstructed into the linearized image. Within each group, linearized retinas were either analyzed separately or averaged into a composite image.

Retinal Thickness—Total (light- and dark-adapted) and postreceptor (light-adapted only) retinal thicknesses were measured from superior and inferior retina at six different locations per side as the radial distance between the anterior and posterior edges of the retina or anterior and border of postreceptor and receptor retina, respectively, at distances between 0.4 and 1 mm from the optic nerve. No differences between superior and inferior retina values were noted (data not shown). Thus, averaged hemiretinal data were used for comparisons.

Layer-Specific Signal Intensity—Postreceptor and receptor retinal signal intensities were analyzed using the program IMAGE (a freeware program available at http://rsb.info.nih.gov/nih-image/; last accessed May 1, 2007) and derived macros.[20] We controlled for changes in receiver gain between animals by setting the signal intensity of a region of noise in each rat to a fixed value. Postreceptor and receptor signal intensity data (from the edge of the optic nerve to 1 mm from the center of the optic nerve) were extracted. Dark- and light-adapted eyes were analyzed as follows. The provisional border between postreceptor and receptor retina was then set at 4 pixels (93.6 μm) posterior to the clearly defined vitreoretinal division. This postreceptor division could be visually confirmed only in light-adapted retinas. We then set the provisional border between retina and choroid at 3 pixels (70.2 μm) posterior to the postreceptor/receptor border. Pixels immediately anterior to the postreceptor/receptor and receptor/choroid borders were considered representative of postreceptor and receptor retina (respectively) and were analyzed as described.

Passive BRB PS′/Gd-DTPA—Blood-retinal barrier permeability surface area product (BRB PS′) was estimated as previously described.[17] Briefly, after coregistration, the MRI data were analyzed using the program IMAGE (a freeware program available at http://rsb.info.nih.gov/nih-image). The three precontrast images were averaged to improve the signal-to-noise ratio. For each pixel, the fractional signal enhancement, E, was calculated as described.[17] A region-of-interest (ROI) was chosen on the E map that contained the entire vitreous space. The area of this ROI and the mean E within the ROI were measured at each postcontrast time point. Only the last four time points (13, 15, 17, and 19 minutes) were converted to BRB PS′ values.[17] These PS′ values were then averaged to minimize the influence of noise on any one PS′ value.

Electrophysiology—Retinal function was assessed at baseline (1 week before) and at 4 hours and 7 days after $MnCl_2$ injections performed as described. Animals were anesthetized under dim red light (λ_{max} = 650 nm) with ketamine (60 mg/kg) and xylazine (5 mg/kg; Troy Laboratory, Frenchs Forest, NSW, Australia), with mydriasis (≥4 mm) and corneal anesthesia induced with tropicamide (Mydriacyl 0.5%; Allergan, Irvine, CA) and proxymetacaine (Ophthetic 0.5%; Allergan), respectively. Signals were recorded with silver-chloride electrodes mounted on the cornea and sclera and referenced to a stainless steel tail electrode (Grass Telefactor, West Warwick, RI). Corneal lubrication was achieved with 1.0% carboxymethylcellulose (Celluvisc; Allergan).

Light stimulation was achieved with brief (1-ms) white flashes from light-emitting diodes (5-W, 5500°K, Luxeon; Phillips Lumileds Lighting Company, San Jose, CA) delivered through a ganzfeld sphere (Photometric Solutions International, Huntingdale, Victoria, Australia). Scotopic luminous exposure (log cd · s · m^{-2}) was measured with a photometer (IL1700; International Light Research, Peabody, MA) with a scotopic luminosity filter (ZIE, scotopic filter) in place. Responses were recorded over a range of stimulus exposure (−5.83 to 1.28 log cd · s · m^{-2}). At dim intensities (less than −5.28 log cd · s · m^{-2}), 20 signals were averaged to improve the signal-to-noise ratio. Fewer signals were averaged at moderate light levels (5–10 repeats), and single responses were recorded with bright flashes (greater than −3.34 log cd · s · m^{-2}). To ensure adequate adaptation between successive flashes, the inter-stimulus interval was lengthened from 5 seconds for the dim flashes to 180 seconds for the brightest flash. Signals were amplified (×1000) and digitized (4 kHz) with band-pass settings of 0.3 to 1000 Hz (−3 dB).

The ERG waveform (Fig. 1) at bright intensities is composed of an initial negative going response (a-wave) followed by a positive postreceptoral deflection (b-wave) on which can be seen small oscillatory potentials (OPs). The a-wave is known to reflect the activity of photoreceptors[21] and can be described using a computational model based on the biochemical cascade of phototransduction as given by Equation 1,[22]

$$P3(i,\ t) = Rm_{P3} \cdot [1 - e^{-i \cdot S \cdot (t - t_d)^2}] \text{ for } t > t_d \quad (1)$$

where the photoreceptor response (*P*3) over time (*t*, *s*) for a given stimulus intensity (*i*, log cd · s · m^{-2}) can be described by a saturated amplitude (Rm_{P3}, μV), a sensitivity parameter (*S*, $cd^{-1} \cdot m^2 \cdot s^{-3}$) and a delay ($t_d$, *s*), which includes both biochemical and recording latencies. The *P*3 model was fitted as an ensemble to the raw data over a range luminous exposures (0.98–1.58 log cd · s · m^{-2}) by floating Rm_{P3} and *S* (with t_d fixed to 3.6 ms) and minimizing the sum-of-square (SS) error (Excel Solver module; Microsoft Excel, Redmond, WA) for all data points from t_d to the a-wave minimum or to a maximum of 18 ms (see Fig. 5B for a fit of the *P*3 model to the raw).

The ON-bipolar cell derived *P*2[23] is the positive component that underlies the b-wave. To expose the *P*2, the modeled *P*3 was subtracted from the raw data.[24] After filtering to remove the OPs (fifth-order Butterworth, −3 dB at 50 and 220 Hz), the amplitude at a fixed criterion time of 120 ms after stimulus onset is extracted. The amplitude intensity response of the *P*2 is described by fitting a Naka-Rushton relationship, which has the same form as a Hill function (Equation 2).

$$V(I) = V_{max}\frac{I^n}{I^n + K^n} \quad (2)$$

The *P*2 amplitude response (V, μV) as a function of stimulus exposure (I, log cd · s · m^{-2}) is given by a maximum amplitude (V_{max}, μV), and a semisaturation parameter (K, log cd · s · m^{-2}, 1/K give the sensitivity). The slope (n) parameter returns a value of 1 for a single underlying cellular generator, with the contributions of inner retinal activity reducing n to less than unity. Oscillatory potentials at the brightest intensity (1.28 log cd · s · m^{-2}) were analyzed by their peak frequency in the Fourier domain and by their summed root-mean-squared amplitude (20–120 ms epoch) and peak time in the time domain.

Statistical Analysis

PS′, retinal thickness, and ERG data were consistent with a normal distribution, and respective comparisons between groups were performed through unpaired (PS′, thickness) or paired (ERG) *t*-test analysis. Comparisons of MEMRI retinal signal intensities were performed using a generalized estimating equation (GEE) approach.[25] GEE performs a general linear regression analysis with all the pixels in each subject and accounts for the within-subject correlation between adjacent pixels. In all cases, two-tailed $P < 0.05$ was considered statistically significant.

Results

Choroid/Gd-DTPA

Before Gd-DTPA, as expected for light-adapted retinas, postreceptor layer signal intensity ($n = 5$; 104.1 ± 1.1 a.u. [mean ± SEM]) was greater ($P < 0.05$) than that for receptor layer (89.4 ± 1.5 a.u.; Fig. 1).[5] After Gd-DTPA administration, signal intensities of postreceptor (103.7 ± 1.5 a.u.) and receptor (95.9 ± 1.7 a.u.) retina did not differ significantly ($P > 0.05$) from those measured before Gd-DTPA.

Subtracting pre-Gd-DTPA images from the post–Gd-DTPA images yielded a presumptive choroidal circulation (Fig. 1) with a thickness of 65.5 ± 7.6 μm ($n = 5$). In a separate study, choroidal thicknesses in the central retina were determined histologically and conservatively corrected for approximately 25% shrinkage (vide infra; Fig. 2). Within the eccentricity range we measured (0.4–1 mm on either side of the optic nerve head), choroidal thickness varied between 25 and 100 μm. The distribution is not uniform (Kolmogorov-Smirnov normality test; $P < 0.01$) because the choroid tends to become gradually thinner and to have more peripheral eccentricities, and we excluded values for eccentricities outside our range (always less than 25 μm). The mean for the resultant distribution was 49.6 ± 6.2 μm.

MEMRI after Intravitreal Injection

After intravitreal injections of PBS, receptor signal intensities were not significantly ($P > 0.5$) different from postreceptor intensities (Fig. 3). Compared with PBS-injected eyes, PBS + ouabain treatment produced subnormal ($P < 0.05$) receptor and postreceptor signal intensities (Fig. 3). To test for similar manganese exposure between the groups, we compared group signal

intensities of extraocular muscle and found no differences ($P > 0.05$; data not shown). Retinal thicknesses after intravitreal injections are compared in Table 1.

MEMRI after Sodium Iodate Treatment

Twenty-four hours after sodium iodate administration, receptor and postreceptor signal intensities were both supernormal ($P < 0.05$; Fig. 4). No statistical difference ($P > 0.05$) was noted in total and postreceptor thickness between control and sodium iodate treated rats (Table 1).

Increased Gd-DTPA in the vitreous was detectable in 5 of 8 treated rats, and these data from leaky retinas were used to calculate BRB permeability. A plot of layer-specific signal intensities and permeability in each retina provided no evidence that receptor and postreceptor MEMRI signal increases were related to increased BRB permeability (Fig. 4B).

Effect of $MnCl_2$ on Retinal Function

Figure 5A shows that little difference can be discerned between waveforms taken over a wide range of light levels from an animal 1 week before and 4 hours after $MnCl_2$ injection. The photoreceptoral response is analyzed by modeling the leading edge of the a-wave shown in Figure 5B. No significant difference ($P > 0.05$) was found between any of the time points assessed in this study for either phototransduction amplitude (Fig. 5C; baseline, −450 ± 31; 4 hours, −457 ± 17; 7 days, −430 ± 28 μV) or sensitivity (Fig. 5D; baseline, 3.41 ± 0.02; 4 hours, 3.45 ± 0.04; 7 days, 3.33 ± 0.03 log $cd^{-1} \cdot m^2 \cdot s^{-3}$). The postreceptoral P2 response was analyzed by modeling the amplitude intensity response function as shown in Figure 6A. The average P2 amplitude (Fig. 6B, V_{max}; baseline, 1108 ± 63; 4 hours, 1104 ± 64; 7 days, 1157 ± 77 μV), semisaturation (Fig. 6C, K; baseline, −3.17 ± 0.03; 4 hours, −3.21 ± 0.05; 7 days, −3.11 ± 0.03 log $cd \cdot s \cdot m^{-2}$), and slope (Fig. 6D, n; baseline, 0.99 ± 0.03; 4 hours, 1.04 ± 0.05; 7 days, 0.97 ± 0.02) were not significantly ($P > 0.05$) affected by systemic $MnCl_2$ injection at 4 hours or 7 days after treatment compared with baseline. Although not shown, analysis of oscillatory potential frequency (baseline, 106.6 ± 2.5; 4 hours, 111.7 ± 2.4; 7 days, 106.5 ± 3.2 Hz), RMS amplitude (baseline, 5.3 ± 0.2; 4 hours, 5.6 ± 0.1; 7 days, 5.4 ± 0.1 μV^2), and peak time (baseline, 33.4 ± 1.0; 4 hours, 31.4 ± 0.9; 7 days, 31.5 ± 1.3 ms) revealed no significant difference between baseline and either postinjection time point ($P > 0.05$ for 4 hours and 7 days).

Intraretinal Clearance and Reproducibility

In control rats treated with a single $MnCl_2$ injection, intraretinal signal enhancement decayed over time (Fig. 7A). The decay portion of the curve could be fit to a simple exponential function with time constants of 1.1 days for receptor retina and 0.69 days for postreceptor retina. In addition, the same group of rats injected with $MnCl_2$ twice (2 weeks apart) yielded no significant difference in intraretinal uptake (Fig. 7B).

Discussion

In this study, we report proof-of-concept that (1) neither the choroidal circulation, damage to the BRB, nor manganese toxicity confounds intraretinal interpretation of MEMRI data; (2) distinct intraretinal manganese uptake patterns are found after metabolic inhibition (ouabain) and RPE layer damage (sodium iodate) following systemic administration of $MnCl_2$; and (3) intraretinal ion demand from a single animal can be measured at multiple time points. The intention of this work was to present feasibility data demonstrating that MEMRI can be used to study retinal anatomy and layer-specific activity in models of ocular insult. Improvements in image signal-to-noise, such as through the use of higher magnetic fields or different coil arrangements, are expected to decrease intraretinal signal intensity variability at any given time

point. Intraretinal ion demand is expected to complement data available from existing techniques, such as ERG and histology. The MEMRI technique has several advantages. Rats are conscious during light and dark adaptation (no confounding anesthetic effects). Activity maps of very high resolution in two dimensions (intraretinally in different retinal layers and panretinally as each layer spans from ora serrata to ora serrata) can be acquired in vivo, contrary to methods such as ERG. Panretinal structure and ion demand information can be simultaneously measured, contrary to methods such as ocular coherence tomography, which typically measures retinal structures over a small retinal region.[26]

At high doses, manganese is toxic.[27] In this study, we show that retinal function assessed with the use of ERG, which reflects change in transmembrane ionic fluxes in response to light, is unaltered at 4 hours after intraperitoneal injection of 44 mg/kg $MnCl_2$. In particular the photoreceptor-driven a-wave, which reflects light-induced depression of the dark current, was unaltered.[21] This outcome suggests that, at the concentration used here, $MnCl_2$ has negligible effect on the phototransduction cascade and those components responsible for the photoreceptor dark current (e.g., outer segment nonspecific cationic channels, inner segment ion pumps, and exchangers). In addition, the dominant inner retinal response, the b-wave, known to involve ON-bipolar cell activity[23,24] and, to some extent, Müller cell ionic buffering, was also unaffected. We also show that the function of these ERG components and the oscillatory potentials continued to be normal after 1 week. The experimental design allowed us to detect a 25% change in ERG amplitudes with a power of 0.93; as such, we believe that the negative finding is a true outcome. Although the potential toxicity of repeated $MnCl_2$ injection required for longitudinal studies must be considered in future studies, the apparently complete clearance of intraretinal manganese (Fig. 7A) suggests that multiple injections of modest doses of manganese will not be toxic. Taken together, these data support our previous conclusion, drawn from 1-month postinjection data, that a single moderate dose of $MnCl_2$ administered systemically does not, in and of itself, produce ocular injury; thus, application of MEMRI to study disease-based damage to the retina is reasonable.[5]

Previously, we found no differences between histology and MRI-derived whole retinal thickness or inner retinal thickness.[5] However, in that earlier work, retina and choroid were not distinguishable and we were unable to determine the contribution of the choroid to MRI assessment of retinal thickness and ion demand.[5,6] To address this issue, the contrast agent, Gd-DTPA, was used to highlight the vascular spaces of the retina. Retinal vessels were not well detected in the present study, possibly because of a combination of low signal noise at the high-resolution acquisition conditions used in this study, the relatively small size of the retinal vessels compared with the choroidal vessels, and partial volume averaging with non-vascularized retina. Nonetheless, subtracting the pre– and post–Gd-DTPA images of each rat clearly revealed a band of enhancement located in the posterior retina, where one would expect the choroidal circulation.

Based on the literature, the choroid is expected to have a thickness in the range of 25 to 45 μm.[8,28–30] In this study, we compared our results to histologically-derived values from eyes perfused with aldehyde fixatives. Comparison of cross-sections from eyes of perfused animals with slices through fresh eyes of the same species (not shown) allowed us to estimate tissue shrinkage due to fixation as approximately 25%. If we account for this degree of shrinkage in our measurement, the mean thickness increases to approximately 50 μm. From the MRI data, choroidal thickness was estimated in two different ways. First, the difference between pre- and post-Gd-DTPA total retinal thickness (Table 1) was calculated. However, this approach produced a choroidal thickness that was much lower (16 μm) than expected. This low thickness estimate was probably due to overlap between choroid and retina by an unknown extent since choroidal boundaries are not observed. In the second approach, the pre- and post-Gd-DTPA images were subtracted first, and then thickness estimated from the remaining signal of the

presumptive choroid. This yielded a choroidal thickness of approximately 65.5 μm. Based on the work of Cheng et al.,[8] we estimate that correcting for partial volume averaging caused by the curvature of the eye and our 620-μm slice thickness could reduce a 65.5-μm choroid thickness to approximately 45 μm (data not shown). Thus, although exact histologic and partial volume correction factors were not determined in this study, rational adjustments of the histology (50 μm) and MRI (45 μm) data produced reasonable agreement between these two methods and with the literature.[8,28,29,31] Furthermore, as seen in Figure 1, it appears that at the resolution used in this study, the choroidal circulation is unlikely to alter the interpretation of intraretinal signal intensity changes.

A promising future application of MEMRI is to follow the progression of retinal injury/disease and treatment efficacy. Because the effects of ouabain inhibition[30] and sodium iodate toxicity are not reversible, time course studies under these conditions were not performed. Instead, we investigated the intraretinal clearance of manganese using nontermination experiments in control rats (Fig. 7A). These data suggest that manganese clearance from the receptor retina was faster than that of the postreceptor retina. In addition, the present data demonstrate that after a single injection of $MnCl_2$, the buildup of intraretinal manganese occurs more quickly than its clearance. This temporal evolution pattern (manganese influx greater than outflux) is similar to that found in brain after systemic administration of $MnCl_2$.[32] The data in Figure 7A also support our interpretation of manganese uptake as a measure of ion demand because probably little manganese is lost by 4 hours after the manganese injection. Once baseline conditions were reached, reasonable reproducibility of intraretinal uptake of manganese was found (Fig. 7B). These data clearly demonstrate the reliability of the MEMRI approach. More work is needed to better understand the mechanism responsible for manganese uptake and clearance. This is a challenging problem because it is likely that many factors can affect manganese flux and distribution.

In this study, we investigated one possible regulator of intraretinal flux: Na^+/K^+-ATPase. Na^+/K^+-ATPase is important to normal vision because it maintains sodium and potassium gradients during dark current generation in the photoreceptors, synaptic activity throughout the retina, action potentials in ganglion cells, and neurotransmitter uptake by Müller cells. Furthermore, Na^+/K^+-ATPase activity accounts for roughly half the metabolic energy used by the retina for active transport of cations across cell membranes.[33,34] Ouabain is a specific inhibitor of Na^+/K^+-ATPase activity and thus can be used to examine acute compromise of ionic flux associated with oxygen or glucose deprivation, or both.[15,35,36]

The present finding of an ouabain-induced reduction in manganese uptake intraretinally seems reasonable. First, high ouabain-affinity Na^+/K^+-ATPase isoforms are located in postreceptor and receptor rodent retina.[37] Second, the present vitreous ouabain concentration after injection (30 μM final vitreal concentration [3 μL of 0.55 mM ouabain injected into a 55-μL rat vitreous[38]]) falls in the range of values (0.4–100 μM) found in the literature that have been shown to be adequate for disrupting intraretinal ion fluxes. Norido et al.[39] found that a vitreous level of approximately 0.4 μM in rabbits in vivo (intravitreal injection of 0.85 nmol ouabain assuming a 2-mL vitreous volume), was associated with a 50% reduction in ERG waves.[30] Winkler[40] found that 100 μM ouabain concentration causes rapid loss of photoreceptor function in an ex vivo retinal preparation. In addition, Weymouth et al. (Weymouth AE, et al. *IOVS* 2004;45:ARVO E-Abstract 1349) reported that after intravitreal injection of ouabain (vitreous level 30 μM) in rats, large reductions in ERG waves and Na^+/K^+-ATPase activity were evident. Third, ouabain-induced reduction in Na^+/K^+-ATPase activity is expected to increase intracellular sodium levels, which in turn, can inhibit Na^+/Ca^{2+}exchanger activity and, we speculate, manganese uptake.[41] Although the presently used dose or schedule of ouabain may not optimally suppress Na^+/K^+-ATPase activity, the procedure used is adequate to address the proof-of-concept goals of this study. Thus, the present data are consistent with expected

ouabain-induced disruption of ion gradients and function in receptor and postreceptor retina and suggest that subnormal MEMRI at least partially reflects the inhibition of Na^+/K^+-ATPase activity. These considerations raise the possibility that MEMRI will be useful in the study of retinopathies associated with suppressed Na^+/K^+-ATPase activity, such as diabetic retinopathy.[9,10]

In this study, we found evidence that retinal thickness after PBS and PBS + ouabain intravitreal injections were different from that of controls (Table 1). The thickness changes in Table 1 are smaller than the pixel size; hence, some caution is needed when interpreting such differences. Previous studies of penetrating injury have reported an immediate retina-wide upregulation of c-*fos* and sustained upregulation of endogenous neurotrophic related factors (e.g., basic fibroblast growth factor) and receptors.[42–45] In addition, increased panretinal blood barrier damage occurs after intraocular surgery that did not involve the retina (i.e., partial lens extraction)[46] and 24 hours after injection of human serum albumin into rat vitreous (data not shown). It is plausible that the apparent increase in retinal thickness after injection is real and may be due to the penetrating injury and/or increased phosphate availability associated with intravitreal injection.

Sodium iodate administration produces RPE damage with subsequent increases in BRB permeability, photoreceptor degeneration, retinal dysfunction and loss of visual behavior.[47] In this study, 62.5% of the rats demonstrated BRB damage by 24 hour after 30 mg/kg intraperitoneal sodium iodate injection. It is likely that longer times after exposure or higher doses of sodium iodate would have produced a greater incidence of BRB damage.[47] We examined whether an intraretinal increase in manganese uptake measured after sodium iodate treatment resulted from an associated increase in BRB permeability. The data argue against increased BRB PS′ as a probable mechanism leading to increased ion demand because receptor and postreceptor MEMRI signal intensities did not increase with increasing BRB permeability.

An alternative explanation for the iodate-induced increase in signal intensity is that it represents an increase in intraretinal ion demand. In support of this view, we note that in cats, intravenous injection of sodium iodate produces substantial intraretinal acidification.[48] In addition, in Royal College of Surgeons (RCS) rats, where photoreceptors degenerate secondarily to RPE dysfunction (similar to what occurs after sodium iodate treatment), there is evidence for increased ion channel permeation in photoreceptors before the appearance of apoptosis.[3] Thus, MEMRI may detect early alterations in retinal ion demand resulting from damage of the RPE layer and maybe useful in the study of experimental models of RPE, and possibly photoreceptor, degeneration.

References

1. Marc RE. Mapping glutamatergic drive in the vertebrate retina with a channel-permeant organic cation. J Comp Neurol 1999;407:47–64. [PubMed: 10213187]
2. Acosta ML, Fletcher EL, Azizoglu S, Foster LE, Farber DB, Kalloniatis M. Early markers of retinal degeneration in rd/rd mice. Mol Vis 2005;11:717–728. [PubMed: 16163270]
3. Kalloniatis M, Tomisich G, Wellard JW, Foster LE. Mapping photoreceptor and postreceptoral labelling patterns using a channel permeable probe (agmatine) during development in the normal and RCS rat retina. Vis Neurosci 2002;19:61–70.
4. Srinivasan VJ, Wojtkowski M, Fujimoto JG, Duker JS. In vivo measurement of retinal physiology with high-speed ultrahigh-resolution optical coherence tomography. Opt Lett 2006;31:2308–22310. [PubMed: 16832468]
5. Berkowitz BA, Roberts R, Goebel DJ, Luan H. Noninvasive and simultaneous imaging of layer-specific retinal functional adaptation by manganese-enhanced MRI. Invest Ophthalmol Vis Sci 2006;47:2668–2674.

6. Luan H, Roberts R, Sniegowski M, Goebel DJ, Berkowitz BA. Retinal thickness and subnormal retinal oxygenation response in experimental diabetic retinopathy. Invest Ophthalmol Vis Sci 2006;47:320–328. [PubMed: 16384980]
7. Berkowitz BA, Roberts R, Luan H, Peysakhov J, Mao X, Thomas KA. Dynamic contrast-enhanced MRI measurements of passive permeability through blood-retinal barrier in diabetic rats. Invest Ophthalmol Vis Sci 2004;45:2391–2398. [PubMed: 15223822]
8. Cheng H, Nair G, Walker TA, et al. Structural and functional MRI reveals multiple retinal layers. Proc Natl Acad Sci USA 2006;103:17525–17530. [PubMed: 17088544]
9. Kern TS, Kowluru RA, Engerman RL. Abnormalities of retinal metabolism in diabetes or galactosemia: ATPases and glutathione. Invest Ophthalmol Vis Sci 1994;35:2962–2967. [PubMed: 8206713]
10. MacGregor LC, Matschinsky FM. Altered retinal metabolism in diabetes, II: measurement of sodium-potassium ATPase and total sodium and potassium in individual retinal layers. J Biol Chem 1986;261:4052–4058.
11. Budzynski E, Wangsa-Wirawan N, Padnick-Silver L, Hatchell D, Linsenmeier R. Intraretinal pH in diabetic cats. Curr Eye Res 2005;30:229–240. [PubMed: 15804749]
12. Lin YJ, Koretsky AP. Manganese ion enhances T1-weighted MRI during brain activation: an approach to direct imaging of brain function. Magn Reson Med 1997;38:378–388.
13. Gong H, Amemiya T. Ultrastructure of retina of manganese-deficient rats. Invest Ophthalmol Vis Sci 1996;37:1967–1974. [PubMed: 8814136]
14. Yu X, Wadghiri YZ, Sanes DH, Turnbull DH. In vivo auditory brain mapping in mice with Mn-enhanced MRI. Nat Neurosci 2005;8:961–968. [PubMed: 15924136]
15. Winkler BS. Relative inhibitory effects of ATP depletion, ouabain and calcium on retinal photoreceptors. Exp Eye Res 1983;36:581–594. [PubMed: 6852134]
16. Ennis SR, Betz AL. Sucrose permeability of the blood-retinal and blood-brain barriers: effects of diabetes, hypertonicity, and iodate. Invest Ophthalmol Vis Sci 1986;27:1095–1102. [PubMed: 3721787]
17. Berkowitz BA, Tofts PS, Sen HA, Ando N, de Juan E Jr. Accurate and precise measurement of blood-retinal barrier breakdown using dynamic Gd-DTPA MRI. Invest Ophthalmol Vis Sci 1992;33:3500–3506. [PubMed: 1464496]
18. Berkowitz BA, Ito Y, Kern TS, McDonald C, Hawkins R. Correction of early subnormal superior hemiretinal DeltaPO(2) predicts therapeutic efficacy in experimental diabetic retinopathy. Invest Ophthalmol Vis Sci 2001;42:2964–2969.
19. Schupp DG, Merkle H, Ellermann JM, Ke Y, Garwood M. Localized detection of glioma glycolysis using edited 1H MRS. Magn Reson Med 1993;30:18–27. [PubMed: 8371670]
20. Berkowitz BA. Adult and newborn rat inner retinal oxygenation during carbogen and 100% oxygen breathing: comparison using magnetic resonance imaging Delta PO2 mapping. Invest Ophthalmol Vis Sci 1996;37:2089–2098.
21. Lamb TD, Pugh EN Jr. A quantitative account of the activation steps involved in phototransduction in amphibian photoreceptors. J Physiol 1992;449:719–758. [PubMed: 1326052]
22. Hood DC, Birch DG. A quantitative measure of the electrical activity of human rod photoreceptors using electroretinography. Vis Neurosci 1990;5:379–387. [PubMed: 2265151]
23. Robson JG, Frishman LJ. Response linearity and kinetics of the cat retina: the bipolar cell component of the dark-adapted electroretinogram. Vis Neurosci 1995;12:837–850. [PubMed: 8924408]
24. Hood DC, Birch DG. Beta wave of the scotopic (rod) electroretinogram as a measure of the activity of human on-bipolar cells. J Opt Soc Am A Opt Image Sci Vis 1996;13:623–633. [PubMed: 8627419]
25. Liang Z. Longitudinal data analysis using generalized linear models. Biometrika 1986;73:13–22.
26. Fukuchi T, Takahashi K, Shou K, Matsumura M. Optical coherence tomography (OCT) findings in normal retina and laser-induced choroidal neovascularization in rats. Graefes Arch Clin Exp Ophthalmol 2001;239:41–46. [PubMed: 11271460]
27. Zatta P, Lucchini R, van Rensburg SJ, Taylor A. The role of metals in neurodegenerative processes: aluminum, manganese, and zinc. Brain Res Bull 2003;62:15–28.
28. Steinle JJ, Pierce JD, Clancy RL, Smith G. Increased ocular blood vessel numbers and sizes following chronic sympathectomy in rat. Exp Eye Res 2002;74:761–768. [PubMed: 12126949]

29. Steinle JJ, Smith PG. Role of adrenergic receptors in vascular remodelling of the rat choroid. Br J Pharmacol 2002;136:730–734. [PubMed: 12086982]
30. Norido F, Canella R, Gorio A. Functional and morphological abnormalities induced by ouabain intoxication of the rabbit retina. Acta Neuropathol (Berl) 1983;62:41–45.
31. Steinle JJ, Smith PG. Sensory but not parasympathetic nerves are required for ocular vascular remodeling following chronic sympathectomy in rat. Auton Neurosci 2003;109:34–41. [PubMed: 14638311]
32. Silva AC, Lee JH, Aoki I, Koretsky AP. Manganese-enhanced magnetic resonance imaging (MEMRI): methodological and practical considerations. NMR Biomed 2004;17:532–543.
33. Ames A III, Li YY, Heher EC, Kimble CR. Energy metabolism of rabbit retina as related to function: high cost of Na^+ transport. J Neurosci 1992;12:840–853. [PubMed: 1312136]
34. Medrano CJ, Fox DA. Oxygen consumption in the rat outer and inner retina: light- and pharmacologically-induced inhibition. Exp Eye Res 1995;61:273–284.
35. Malek SA, Adorante JS, Stys PK. Differential effects of Na-K-ATPase pump inhibition, chemical anoxia, and glycolytic blockade on membrane potential of rat optic nerve. Brain Res 2005;1037:171–179.
36. Blanco G, Mercer RW. Isozymes of the Na-K-ATPase: heterogeneity in structure, diversity in function. Am J Physiol 1998;275(pt 2):F633–F650. [PubMed: 9815123]
37. Wetzel RK, Arystarkhova E, Sweadner KJ. Cellular and subcellular specification of Na,K-ATPase alpha and beta isoforms in the post-natal development of mouse retina. J Neurosci 1999;19:9878–9889. [PubMed: 10559397]
38. Berkowitz BA, Lukaszew RA, Mullins CM, Penn JS. Impaired hyaloidal circulation function and uncoordinated ocular growth patterns in experimental retinopathy of prematurity. Invest Ophthalmol Vis Sci 1998;39:391–396. [PubMed: 9477999]
39. Maurice DM. Flow of water between aqueous and vitreous compartments in the rabbit eye. Am J Physiol 1987;252(pt 2):F104–F108. [PubMed: 3812693]
40. Winkler BS. Glycolytic and oxidative metabolism in relation to retinal function. J Gen Physiol 1981;77:667–692. [PubMed: 6267165]
41. Moore ED, Etter EF, Philipson KD, et al. Coupling of the Na^+/Ca^{2+} exchanger, Na^+/K^+ pump and sarcoplasmic reticulum in smooth muscle. Nature 1993;365:657–660. [PubMed: 8413629]
42. Cao W, Li F, Steinberg RH, Lavail MM. Development of normal and injury-induced gene expression of aFGF, bFGF, CNTF, BDNF, GFAP and IGF-I in the rat retina. Exp Eye Res 2001;72:591–604.
43. Ozaki S, Radeke MJ, Anderson DH. Rapid upregulation of fibroblast growth factor receptor 1 (flg) by rat photoreceptor cells after injury. Invest Ophthalmol Vis Sci 2000;41:568–579. [PubMed: 10670490]
44. Penn JS, McCollum GW, Barnett JM, Werdich XQ, Koepke KA, Rajaratnam VS. Angiostatic effect of penetrating ocular injury: role of pigment epithelium-derived factor. Invest Ophthalmol Vis Sci 2006;47:405–414. [PubMed: 16384991]
45. Stitt AW, Graham D, Gardiner TA. Ocular wounding prevents pre-retinal neovascularization and upregulates PEDF expression in the inner retina. Mol Vis 2004;10:432–438.
46. Liu H, Demetriades AM, Xiao WH, Campochiaro PA, Vinores SA. Mouse model of post-surgical breakdown of the blood-retinal barrier. Curr Eye Res 2004;28:421–426. [PubMed: 15512950]
47. Enzmann V, Row BW, Yamauchi Y, et al. Behavioral and anatomical abnormalities in a sodium iodate-induced model of retinal pigment epithelium degeneration. Exp Eye Res 2006;82:441– 448.
48. Yamamoto F, Honda Y. Effects of intravenous iodoacetate and iodate on pH outside rod photoreceptors in the cat retina. Invest Ophthalmol Vis Sci 1993;34:2009–2017.

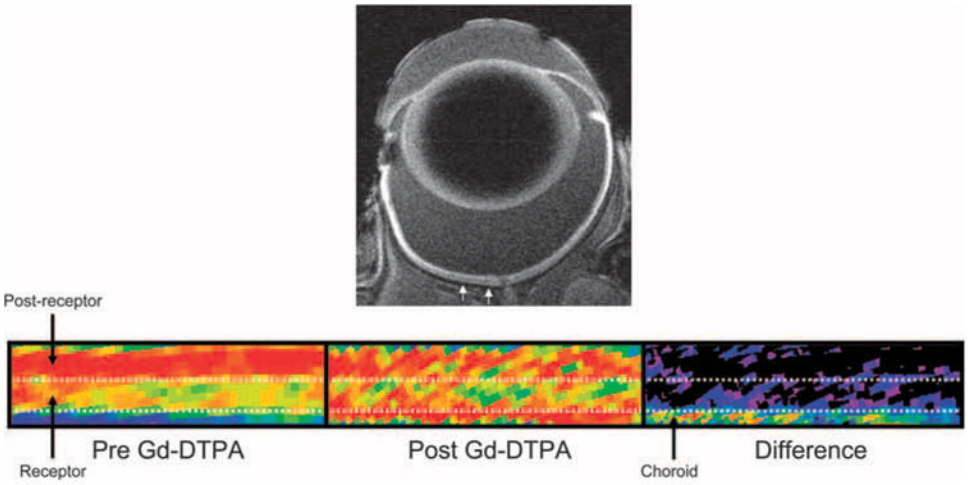

Figure 1.

Top: representative high-resolution MRI image of rat eye 4 hours after intraperitoneal $MnCl_2$ injection. *Small white arrows*: region in superior retina from which linearized pseudocolor images (*bottom*) are derived. *Bottom*: representative regions-of-interest from the same rat before Gd-DTPA (*left*), after Gd-DTPA (*middle*), and the difference (*right*). The same pseudocolor scale was used for all three linearized images, where *blue* to *green* to *yellow* to *red* represent lowest to highest signal intensity. *Uupper dotted white line*: boundary between postreceptor and receptor retina of the control retinas demonstrated in previous studies.[5,6] *Bottom dotted white line*: boundary of the posterior aspect of the control retinas. These data suggest a minimal choroidal contribution to intraretinal analysis.

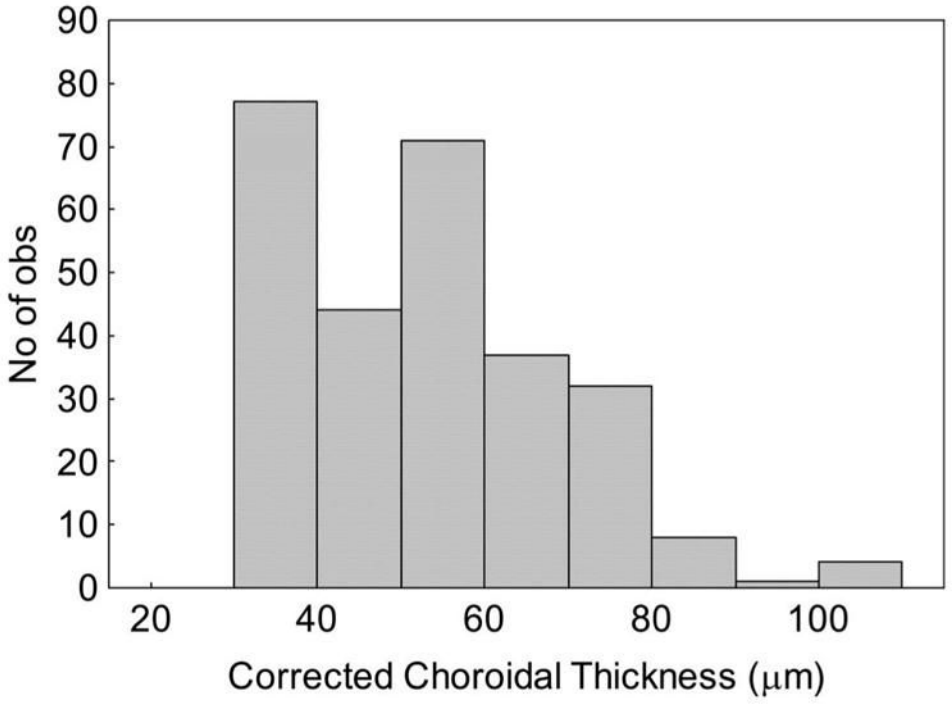

Figure 2.

Histogram of measurements of corrected central choroidal thickness from cross-sections through four eyes of Brown Norway rats transcardially perfused with 4% paraformaldehyde. Values are increased by 25% to correct for tissue shrinkage during fixation. The distribution is not uniform because the choroid becomes thinner as peripheral eccentricities are approached.

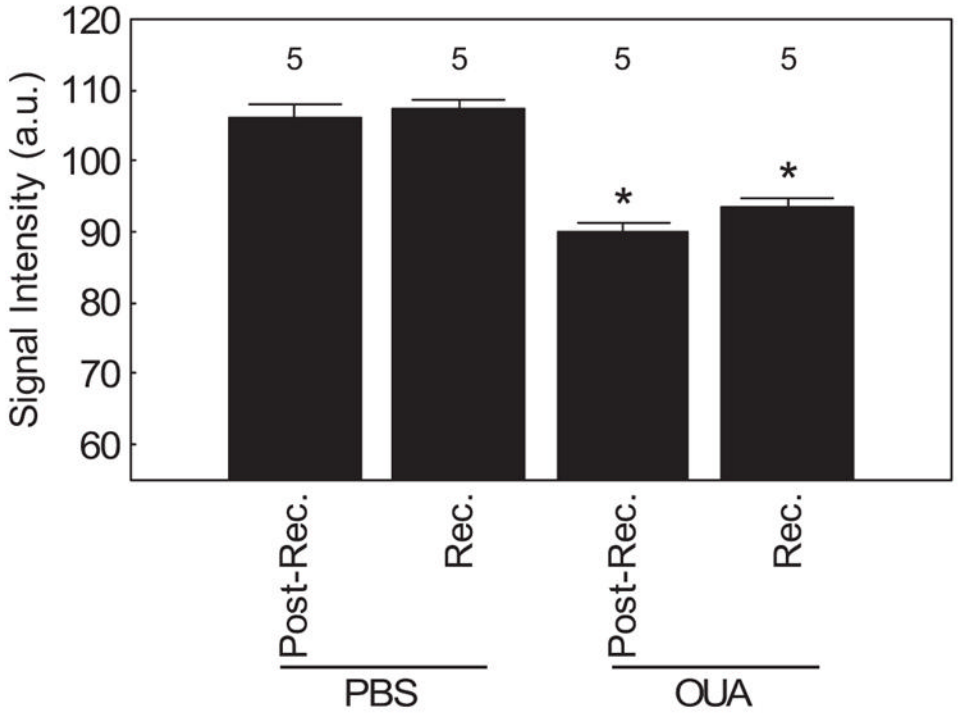

Figure 3.
MEMRI signal intensity changes in receptor (Rec.) and postreceptor (Post-Rec.) retina PBS-injected eyes (PBS) and ouabain-injected eyes (OUA) measured 4 hours after intraperitoneal systemic administration of $MnCl_2$ from the region defined in Figure 1. *Solid bars*: dark-adapted groups. Significant differences between PBS-injected eyes and ouabain-injected eyes (*$P <$ 0.05) were found. Note that the minimum value of the *y*-axis is set to the signal intensity measured in the absence of manganese exposure (i.e., 55).[5] Error bars represent SEM, and numbers above the bars give the number of animals studied.

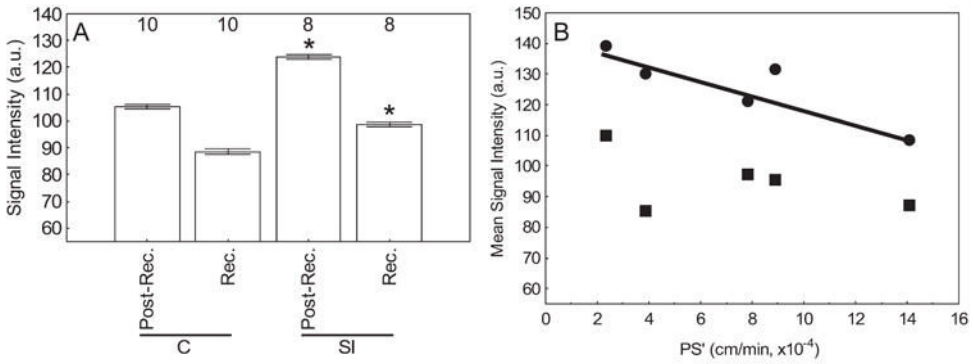

Figure 4.

(**A**) MEMRI signal intensity changes in receptor (rec.) and postreceptor (post-rec.) retina in control (C) and sodium iodate (SI)–treated rats measured 4 hours after intraperitoneal systemic administration of $MnCl_2$ from the regions defined in Figure 1. *Open bars*: light-adapted groups. Significant differences (*$P < 0.05$) were noted. Note that the minimum value of the *y*-axis is set to signal intensity measured in the absence of manganese exposure (i.e., 55).[5] Error bars represent SEM, and numbers above the bars give the number of animals studied. (**B**) Plot of BRB PS′versus MEMRI signal intensity changes in receptor (■) and postreceptor (●) for each rat. A significant negative correlation between BRB PS′ and MEMRI signal was found only for the receptor layer ($r^2 = 0.78$; $P < 0.05$) and not the postreceptor layer ($r^2 = 0.25$; $P > 0.05$). The lack of correlation in the postreceptor retina may be attributed to its lower signal-to-noise ratio than in the receptor layer. In any event, after sodium iodate exposure, retinal manganese uptake did not increase with increasing BRB PS′.

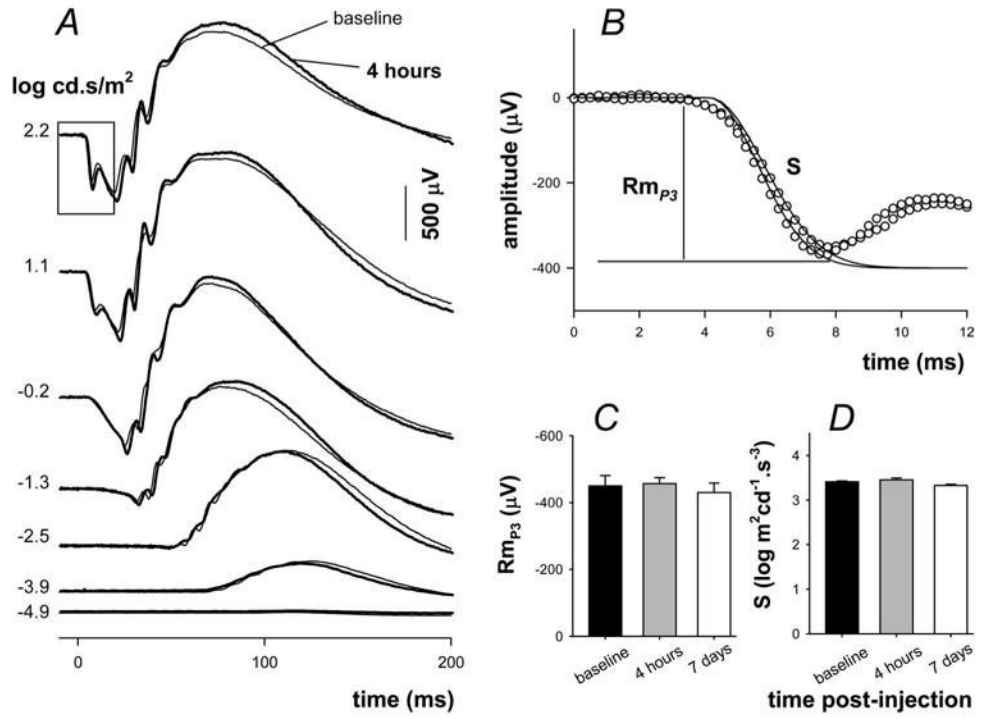

Figure 5.

Effect of $MnCl_2$ injection on retinal function. (**A**) Signals collected 1 week before (*thin traces*) and 4 hours after (*thick traces*) drug treatment. Stimulus exposure is given on the *left*. (**B**) The leading edge of the photoreceptor response (*box*, **A**) is modeled according to a delayed Gaussian model (*traces*) of phototransduction (P3) to give phototransduction amplitude (Rm_{P3}) and sensitivity (S). (**C**) Average (± SEM; $n = 6$) Rm_{P3} 1 week before (*filled*), 4 hours after (*gray*, $n = 6$), and 7 days after (*unfilled*, $n = 6$) intraperitoneal injection of $MnCl_2$. (**D**) Average (± SEM) phototransduction sensitivity for the same time periods.

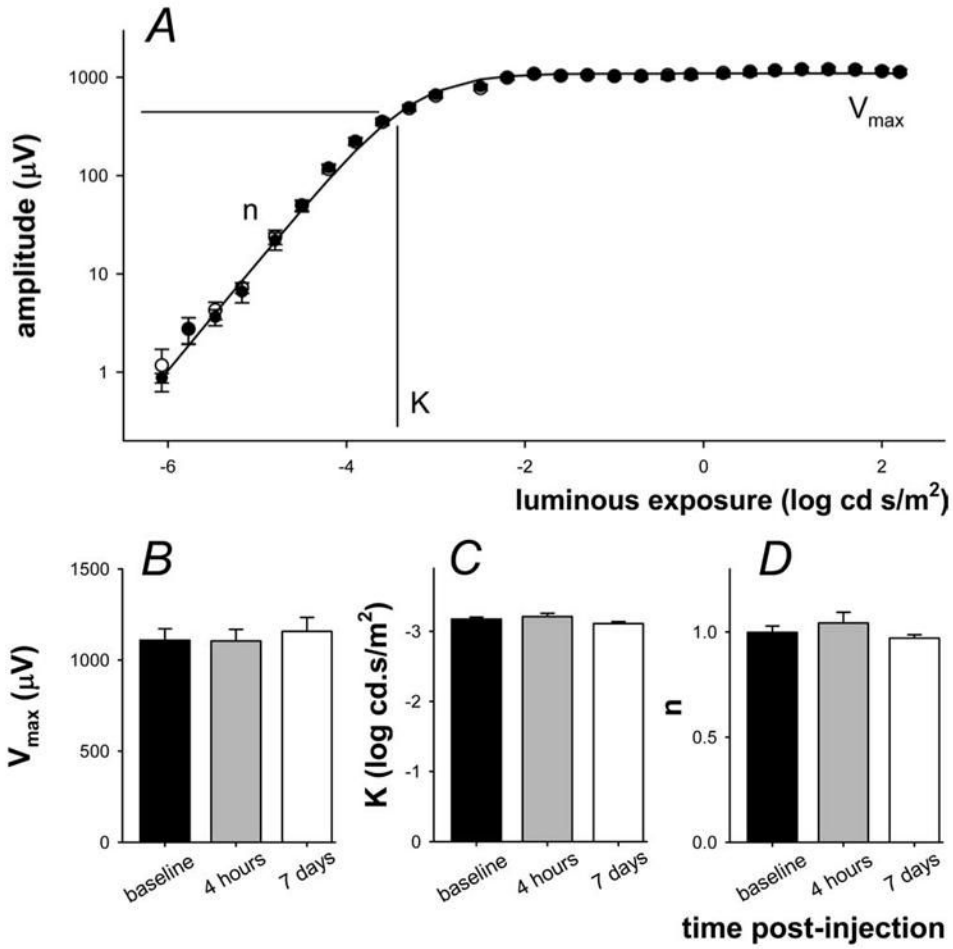

Figure 6.

Effect of $MnCl_2$ injection on the postreceptor (P2) intensity response function. (**A**) The amplitude of the inner retinal P2 (raw – *P*3) was assessed by extracting the amplitude at a fixed criterion time of 110 ms. Average (± SEM) data are shown for signals collected at baseline (*unfilled*, $n = 6$) and 4 hours after injection (*filled*). Intensity response functions are described using a Naka-Rushton function to give saturated amplitude (V_{max}), semisaturation (*K*), and slope (n). (**B**) Average (± SEM) V_{max} 1 week before (*filled*) and 4 hours (*gray*) and 7 days (*unfilled*) after IP injection of $MnCl_2$. (**C**) Average (± SEM) semisaturation. (**D**) Average (± SEM) slope.

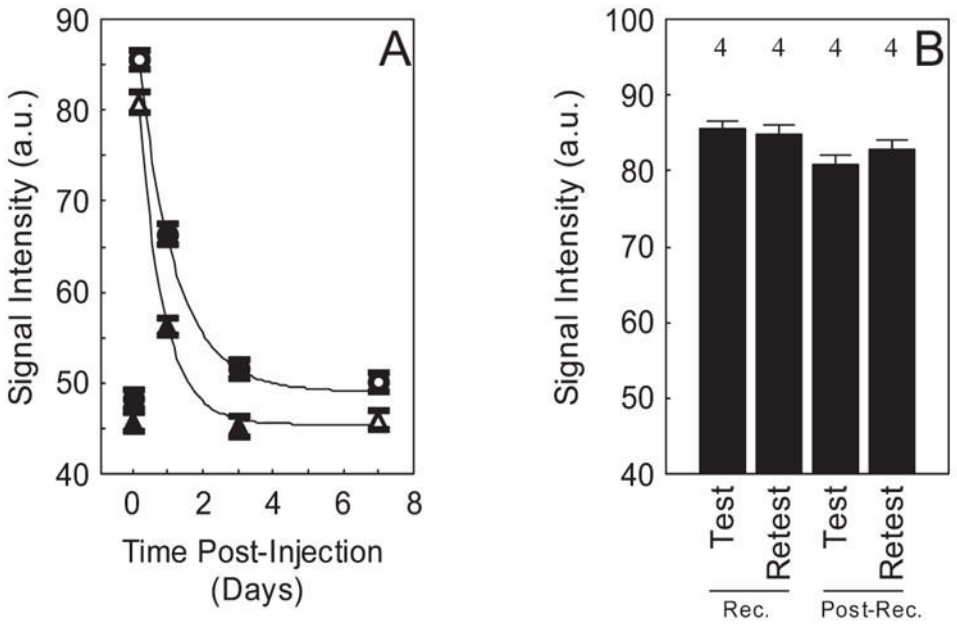

Figure 7.

(**A**) Time course of mean manganese enhancement and clearance in receptor (●) and postreceptor (▲) retina before (time = 0) and after a single IP $MnCl_2$ injection in dark-adapted rats. *Solid lines*: best-fit curves to the data using a three-parameter exponential decay model. *Open symbols*: average data from the same group of rats (n = 4). Mean data from two other groups of rats are also presented: baseline (n = 4) and days 1 and 3 (n = 3) after manganese injection. (**B**) Reproducibility of receptor (Rec.) and postreceptor (Post-Rec.) manganese enhancement in same group of rats indicated by the *open symbols* in (**A**) but given a second $MnCl_2$ injection 2 weeks after the first injection (retest). Error bars represent SEM, and numbers above the bars give the number of animals studied.

Table 1

Summary of Retinal Thickness

Condition	Total Thickness (μm)	Postreceptor Thickness (μm)
Pre-Gd-DTPA (*n* = 5)	201.4 ± 10.6	102.6 ± 6.8
Post-Gd-DTPA (*n* = 5)	217.4 ± 16.1*	103.5 ± 6.7
PBS (*n* = 5)	219.3 ± 11.9*	–
PBS + ouabain (*n* = 5)	214.1 ± 4.8*	–
Sodium iodate (*n* = 8)	203.4 ± 5.8	97.6 ± 6.5

Values are expressed as mean ± SD.

* $P < 0.05$ compared with pre-Gd-DTPA values.